# Solvothermal synthesis, temperature-dependent structural study and magnetic characterization of a multipolydentate oxamate-based 2D coordination network

Ang Li, Lise-Marie Chamoreau, Benoît Baptiste, Ludovic Delbes, Yanling Li, Francesc Lloret, Yves Journaux, Laurent Lisnard

# Solvothermal synthesis, temperature-dependent structural study and magnetic characterization of a multi-polydentate oxamate-based 2D coordination network.

*Ang Li,[#] Lise-Marie Chamoreau,[#] Benoît Baptiste,[§] Ludovic Delbes,[§] Yanling Li,[#] Francesc Lloret,[‡] Yves Journaux,[#] and Laurent Lisnard[#]*.*

# Sorbonne Université, CNRS, Institut Parisien de Chimie Moléculaire, IPCM, F-75252, Paris, France.

§ Sorbonne Université, CNRS, IRD, MNHN, Institut de Minéralogie, de Physique des Matériaux et de Cosmochimie, IMPMC, F-75252, Paris, France

‡ Departament de Química Inorgànica/ Instituto de Ciencia Molecular (ICMol), Facultat de Química de la Universitat de València, València, Paterna, Spain 46980.

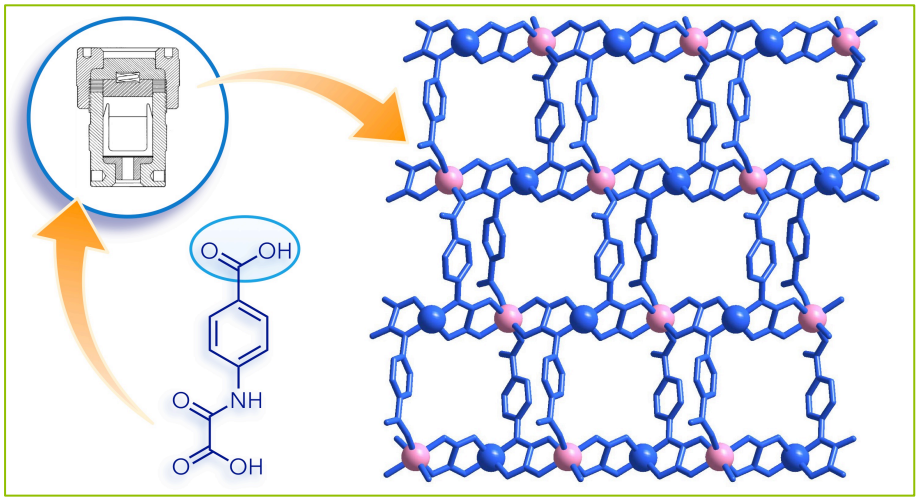


## ABSTRACT.

A multi-polydentate *N*-substituted oxamate ligand bearing an additional carboxylato group has been successfully reacted in solvothermal conditions to form the 2D coordination network $(TMA)_3[CuMn(paba)_2(OAc)]\cdot 8H_2O$ (**1**). This coordination network displays a brick-wall type morphology with, thanks to the augmented connectivity of the ligand, a lower than usual metal ion nuclearity for the building sub-unit. Temperature-dependent structural studies indicate that the layered structure undergoes dehydration at 90°C and remain stable up to 200°C. Magnetic characterizations show that **1** behaves as a ferrimagnet, with a Curie temperature of 2.8 K.

## INTRODUCTION.

Oxamate ligands constitute a remarkable family of ligands for the preparation of appealing molecular materials, such as sieves, sensors or nanoreactors.[1–3] They also play an important role in the design and synthesis of molecular magnetic materials,[4–7] successfully leading to the preparation of single-molecule magnets,[8] spintronic candidates,[9] single-chain magnets,[10] supramolecular magnets,[11,12] 2D/3D coordination network magnets,[13,14] and porous magnets.[15–17] This ability the oxamate ligands have in facilitating the preparation of magnetic molecular materials originates from the unique combination of two features. First, the dissymmetric bis-bidentate nature of the ligand that allows the formation of ferrimagnetic heterobimetallic pairs. Second, the considerable amount of substituents with which it is possible to derive the oxamato group.

One particular group of substituents that shows appeal for the synthetic challenge it represents is the group of substituents bearing an additional coordinating group, different from the oxamate. Investigating the reactivity of these multi-polydentate ligands will further expand the morphology of the coordination architectures it is possible to generate and access with oxamate ligands. For example, the use of amino-acid based oxamate ligands gives access to new porous frameworks with remarkable properties.[18–21] On the other hand, phenolic and benzoic derivatives of the oxamate ligands seem to pose a greater synthetic challenge for the observation of fully coordinating ligands and/or the preparation of heterometallic systems.[22–29] Following our work on the 2-hydroxyphenyloxamate ligand in bench conditions,[29] we had investigated solvothermal conditions to succeed in crystallizing copper(II)-based heterobimetalic compounds. This proved efficient with both the 2-hydroxyphenyloxamate and the 2-carboxyphenyloxamate, yet only 1D coordination polymers were obtained.[30,31] To increase the dimensionality of our edifices, we have naturally moved to a *para*-substitued phenyloxamate, and started to investigate the 4-(ethyloxamate)benzoic acid, $H_2$Et-paba. We present here its use in solvothermal conditions and in the presence of copper(II) to prepare the heterobimetallic $(TMA)_3[CuMn(paba)_2(OAc)]\cdot 8H_2O$ (**1**) 2D coordination network.

## EXPERIMENTAL SECTION.

*Materials and methods.* All reagents were used as purchased with no further purification. The ester form of the ligand, 4-(ethyloxamate)benzoic acid, $H_2$Et-paba, was prepared according to the general procedure for oxamate ligand,[32] which differs from the previously reported synthesis.[26] Magnetic measurements in dc mode were performed on the polycrystalline samples of **1** and **1b** restrained within a capsule with a Quantum Design MPMS SQUID. The ac (alternative current) magnetizations were measured on a Quantum Design PPMS-9T magnetometer. Magnetic susceptibility data were corrected for the diamagnetism of the constituent atoms using the Pascal's constants. The diamagnetism of the sample holder was measured and subtracted from the raw data. NMR spectra were performed on a 400 MHz Bruker AVANCE spectrometer in the "Plateforme RMN Moléculaire / IPCM-Sorbonne Université". Elemental analysis was performed in the "service de microanalyse" at ICSN (CNRS, Gif/Yvette, France) and via the PARI program at the IPGP (Paris, France). ATR/FT-IR spectra were collected on a Bruker TENSOR 27 equipped with a simple reflexion ATR diamond plate of the Harrick MPV2 series. The thermogravimetric analysis (TGA) was performed on a TA Instruments SDTQ600 under air or nitrogen with a heating rate of 5 °C/min.

*Synthesis.* *Synthesis of $H_2$Et-paba, 4-(ethyloxamate)benzoic acid.* To 6.0 g of 4-aminobenzoic acid (M=137.14 $gmol^{-1}$, 43.75 mmol) in 250 mL of THF were added dropwise 5.5 mL of ethyloxalyl chloride (98%; 1.1eq.) under strong stirring. The mixture was refluxed for 90 min and filtered on paper while hot. The removal of the solvent under reduced pressure yielded a white powder. The powder was washed with 200 mL of $H_2O$ under stirring for 60 min and then collected on a sintered glass filter.

Further washing was done with cold 96% ethanol and the solid was dried with ether and then in air. The final product was collected as a white powder (9.41 g, Yield: 90.7%, M=237.2 gmol$^{-1}$). $^{1}$H-NMR (400 MHz, DMSO) δ (ppm): 12.82 (s, 1H), 11.02 (s, 1H), 7.95 (d, 8.0 Hz, 2H), 7.88 (d, 8.0 Hz, 2H), 4.31 (q, *J* = 6.9 Hz, 2H), 1.31 (t, *J* = 7.0 Hz, 3H). $^{13}$C-NMR (101 MHz, DMSO) δ (ppm): 166.39 (s, -COOH), 159.95 (s, -CO-), 155.44 (s, -CONH-), 141.08 (s, Ph), 129.84 (s, Ph), 126.24 (s, Ph), 119.46 (s, Ph), 62.13 (s, -$CH_2$-), 13.41 (s, -$CH_3$). FTIR (cm$^{-1}$): 3332 (m), 2536 (w), 1706 (s), 1676 (s), 1593 (m), 1539 (m), 1419 (m), 1371 (m), 1286 (s), 1169 (s), 1112 (m), 1012 (m), 938 (m), 874 (m), 847 (m), 811 (w), 775 (m), 764 (m), 710 (s), 640 (w), 546 (m), 490 (s), 325 (m). Elemental analysis (%): calc. for $C_{11}H_{11}NO_5$. C, 55.69; H, 4.67; N, 5.90. Found: C, 55.74; H, 4.71; N, 5.95.

*Synthesis of H(TMA)$_2$-paba·1.5H$_2$O, 4-(oxamate)benzoic acid hydrate, mixed tetramethylammonium salt*. To 3.0 g of $H_2$Et-paba (M=237.2 gmol$^{-1}$; 12.6 mmol) suspended in 300 mL of MeOH were added slowly 10.5 mL of TMAOH (2eq., 25% w/w in MeOH). The solution was stirred for 30 min and filtered on paper. Removal of the solvent under reduced pressure yielded the final product as a white solid, dried and kept in a desiccator. (3.14 g, Yield: 62.4%, M=382.45 gmol$^{-1}$). $^{1}$H-NMR (400 MHz, DMSO) δ (ppm): 9.92 (s, 1H), 7.70 (d, *J* = 8.3 Hz, 2H), 7.52 (d, *J* = 8.3 Hz, 2H), 3.13 (s, 24H). $^{13}$C-NMR (75 MHz, DMSO) δ (ppm): 168.60(s, -COO-), 165.00 (s, oxamatic –COO-), 163.06 (s, -CONH-), 139.37 (s, Ph), 137.18 (s, Ph), 129.81 (s, Ph), 117.56 (s, Ph), 54.79 – 54.69 (t, -$NCH_3$). FTIR (cm$^{-1}$): 3301 (w), 3027(m), 1699 (w), 1653(w), 1598(s), 1513(m), 1485 (s), 1402 (w), 1355 (s), 1302 (s), 1244 (m), 1174 (w), 1151 (w), 1104 (w), 1018 (w), 951 (m), 877 (m), 789 (m), 758 (sd), 702 (w), 480 (m), 458 (m), 428 (m), 364 (s), 309 (m), 229 (w). Elemental analysis (%): calc. for $C_{17}H_{32}N_3O_{6.5}$. C, 53.38; H, 8.43; N, 10.98. Found: C, 52.98; H, 8.92; N, 11.49.

*Synthesis of (TMA)$_3$[CuMn(paba)$_2$(OAc)]·8H$_2$O* (**1**). H(TMA)$_2$-paba·1.5$H_2$O (0.95 mmol, 356 mg), Cu(OAc)$_2$.$H_2$O (0.5 mmol, 99 mg), Mn(OAc)$_2$.4$H_2$O (0.5 mmol, 122 mg) and 0.36 mL of TMAOH (25% wt. in water, 1 eq.) were placed in a 23 mL Teflon-lined autoclave reactor filled with DMF (4 mL). The reactor was heated to 120 °C in 2 h, kept at this temperature for 12 h and then cooled down to room temperature in 10 h. Green crystals of **1** were collected and washed with EtOH for single-crystal X-ray diffraction studies. Further washing was done by sonication in EtOH prior to all other characterizations. Yield: 135 mg, 30% (based on H(TMA)$_2$-paba·1.5$H_2$O, M=956,3 gmol$^{-1}$). Elemental analysis (%): calc. for $C_{32}H_{63}CuMnN_5O_{20}$: C, 40.19; H, 6.63; N, 7.32; Mn, 5.74; Cu, 6.64 (wt. Cu/Mn=1.16). Found: C, 40.44; H, 5.85; N, 7.31; Mn, 5.73; Cu, 6.61 (wt. Cu/Mn=1.15). Selected IR data (cm$^{-1}$): 3372(sd), 1627(s), 1583(s), 1559(s), 1486(m), 1373(s), 1334(s), 1168(s), 1099(w), 1016(w), 949(s), 880(w), 841(w), 797(m), 778(s), 707(w), 663(s), 526(w), 496(w), 437 (w).

*Crystallography.* The single-crystal X-Ray diffraction data collection for **1** was carried out at the CRISTAL beamline (synchrotron SOLEIL, Paris) using the synchrotron radiation source (l = 0.67173 Å) with a crystal-to-detector distance of 80 mm. The temperature of the data collection (*T* = 100 K) was reached with a gas streamer (CryoIndustries of America). The wavelength was selected with a double crystal monochromator (Si 111 crystals) and sagittal (horizontal) focalisation was achieved by bending the second crystal of the monochromator. The beam attenuation was performed using Al (or Cu) foils of different thicknesses inserted in the incident beam. Data collection strategies were generated with the CrysAlisPro CCD package. The refinement of the unit cell parameters and data reduction were carried out with CrysAlisPro RED.[33] After the absorption correction, the measured reflections were sorted, scaled and merged by using the SORTAV program.[34,35] The single-crystal X-Ray diffraction data collection for **1b** was carried out on a Bruker Kappa-APEX II CCD diffractometer. Crystals were mounted on a MitiGen Cryomount and placed in the cold flow produced with an Oxford Cryosystems device. Data collection strategies were generated with the APEX2 suite of programs (BRUKER).[36] The refinement of the unit cell parameters and data reduction were carried out with SAINT (BRUKER),[36] and absorptions were corrected with SADABS.[35,36] The structures of **1** and **1b** were solved with SHELXT-14[37] and refined with the SHELXL-2014/7 program[38] in the OLEX2 software.[39] For

compound **1** all non H atoms were refined with anisotropic displacement parameters, RIGU and a few geometrical restraints were applied on the disordered tetramethyl ammonium. For **1b** due to the low data/parameter ratio and the limited resolution, RIGU restraints were introduced for aromatic rings of the paba ligands and for all ammonium cations to allow the anisotropic refinement of atoms. Crystallographic parameters and data refinement results for **1** and **1b** are given in Table 1. CCDC-2194184-2194185 contain the supplementary crystallographic data for this article. The data can be obtained free of charge from The Cambridge Crystallographic Data Centre via www.ccdc.cam.ac.uk/structures. The X-ray powder diffraction (XRD) patterns were collected at the X-ray diffraction platform of the IMPMC, from samples deposited on zero background silicon holders, using an X'Pert Pro MPD Panalytical diffractometer in Bragg-Brentano geometry equipped with a Co–Kα radiation source ($l_{K\alpha1}$ = 1.78897 Å, $l_{K\alpha2}$ = 1.79285 Å) and an X'Celerator detector. Rietveld refinements were performed with the FullProf suite of programs.[40,41] Crystal structures of **1** and **1b** were used as starting datasets for the refinement at room temperature and at 90 °C. The first peak discrepancy in the diagram of **1** comes from difficulties in correctly modeling the strong asymmetry at low angles. Thermodiffraction measurements were performed on the same diffractometer equipped with a Anton Paar HTK 1200 N oven and using a 80 mL/min nitrogen flow.

Table 1. Crystallographic parameters and data refinement for **1** and **1b**.

| | **1** | **1b** |
|---|---|---|
| Formula | $C_{32}H_{55}CuMnN_5O_{16}$ | $C_{32}H_{47}CuMnN_5O_{12}$ |
| FW [g mol$^{-1}$] | 884.29 | 812.22 |
| Crystal system | Monoclinic | Monoclinic |
| Space group | $P2_1/n$ | $P2_1/c$ |
| *a* [Å] | 9.5588(4) | 9.2684(16) |
| *b* [Å] | 24.6546(12) | 23.132(4) |
| *c* [Å] | 17.5097(5) | 17.948(3) |
| $\beta$ [°] | 96.887(4) | 101.351(8) |
| *V* [Å$^3$] | 4096.7(3) | 3772.7(11) |
| *Z* | 4 | 4 |
| *T* [K] | 100(2) | 365(2) |
| $\lambda$ [Å] | 0,67173 (SR) | 1.54178 (Cu-Ka) |
| $\rho_{calc}$ [g cm$^{-3}$] | 1.434 | 1.430 |
| $\mu$ [mm$^{-1}$] | 0.894 | 3.975 |
| F(000) | 1856 | 1696 |
| Crystal size [mm] | 0.04x0.02x0.01 | 0.04x0.02x0.02 |
| *q* limits [°] | 2.17-19.62 | 3.15-40.42 |
| Measured reflections | 17780 | 15743 |
| Unique reflections | 4283 | 2305 |
| $R_{int}$ | 0.1087 | 0.1769 |
| Reflections I>2σ(I) | 2814 | 1107 |
| Parameters | 507 | 465 |
| Restraints | 96 | 250 |
| $R_1$ [I>2σ(I)] | 0.0674 | 0.0690 |
| $wR_2$ | 0.1730 | 0.1996 |
| GOF | 1.041 | 1.030 |
| Largest residuals [eÅ$^3$] | -0.52;1.42 | -0.454;0.529 |
| CCDC deposition # | 2194184 | 2194185 |

$$R_1 = \frac{\sum||F_0| - |F_c||}{\sum|F_0|} \qquad \omega R_2 = \sqrt{\frac{\sum(\omega(F_0^2 - F_c^2)^2)}{\sum(\omega(F_0^2)^2)}}$$

## RESULTS AND DISCUSSION.

Compound **1** was synthesized solvothermally from the tetramethylammonium acidic salt of the $(paba)^{3-}$ ligand, $H(TMA)_2$-paba·$1.5H_2O$, with metal ion acetate salts, in DMF and in the presence of one equivalent of TMAOH. **1** crystallizes in the monoclinic $P2_1/n$ space group and its structure consists of the anionic $\{Mn^{II}\text{-}Cu^{II}\}$ 2D network $[CuMn(paba)_2(OAc)]^{3-}$, tetramethylammonium $(TMA)^+$ counter-cations and water crystallization molecules. The Cu(II) ion (Cu1) is five-coordinate in a square pyramidal environment (Figure 1). Two $(paba)^{3-}$ ligands bind the copper center in a *cis* fashion, each via one nitrogen atom and one oxygen atom from their oxamate group (N1,O1; N2,O6). One oxygen atom (O11) coming from a mono-coordinated acetate anion completes the coordination sphere of the copper ion. Two nitrogen atoms and one oxygen atom (O1) from the ligands, as well as the oxygen atom from the acetato group define the square base of the pyramidal environment. The bond lengths in this plane range from 1.967(6) to 2.029(5) Å, with the shortest distances found for the Cu—N bonds. The apical position is defined by one oxamate oxygen atom (O6), at 2.186(5) Å. The geometry of the Cu(II) ion is distorted, with N/O—Cu—N/O angles varying from 80 to 100° (av. deviation to orthogonality of 6°), and a twisted square base (N1–Cu1–O7/N2–Cu1–O4 dihedral angle: 15°). As a result, and despite the *cis* coordination of the ligands, the angle formed by the position of the $(paba)^{3-}$ ligands' pendent carboxylate arms is closer to 180° than to 90°. Indeed, the (OO)C–Cu–C(OO) angle is 144°. The two ligands also show different conformations. The dihedral angles between the planes described by the phenyl rings and the oxamato groups are found at 88 and 30° (around N1 and N2 respectively). However, with the *cis* coordination of the ligands and the distortion of the Cu(II) ion geometry, the dihedral angles between the phenyl rings and the square base of the metal ion are similar, 86 and 88°. The Mn(II) ion is six-coordinate with a distorted octahedral surrounding. The metallic center is *cis*-coordinated by the remaining four carbonyl groups of two oxamate ligands (O2, O3, O7, O8) and by two mono-coordinated carboxylato groups (O4, O10) coming from another two $(paba)^{3-}$ ligands. The Mn—O distances range from 2.114(6) to 2.226(5) and average 2.167 Å. The O–Mn–O angles vary from 75 to 102° with an averaged deviation to orthogonality of 5°. BVS calculations support the presence of Mn(II) ions (See Supporting Information). **1** is the first structural example of the {paba} ligand in its fully deprotonated form and adopting a bis-bidentate bridging coordination mode for the oxamato group. In the previously reported compounds prepared in bench conditions from $H_2$Et-paba,[26–28] the oxamate function remains protonated, i.e. non-bridging or non-coordinating (Scheme 1).

Considering the $[Cu(paba)_2]^{4-}$ in-situ formed metalloligand, its coordination via the oxamate bridges to the Mn(II) ions gives a zig-zag chain (Mn–Cu–Mn = 119°) along the crystallographic *a* axis, with the pendent *para*-substituted phenyl carboxylato groups roughly aligned along *c* (Figure 2). These carboxylato groups then bind manganese ions from adjacent chains to yield a corrugated 2D brick-wall structure for **1** (Figure 2). The concomitant role of solvothermal conditions and use of copper(II) ions should be stressed in the formation and crystal growth of a 2D network, thanks to an almost fully coordinating $(paba)^{3-}$ ligand. In bench conditions, the presence in this ligand of non-coordinating N/O donor atoms limited its connectivity, and resulted in either 0D (M = Fe(II), Cu(II)) or 1D compounds (M = Mn(II), Co(II), Zn(II), Eu(III), Tb(III), Gd(III)).[26–28]

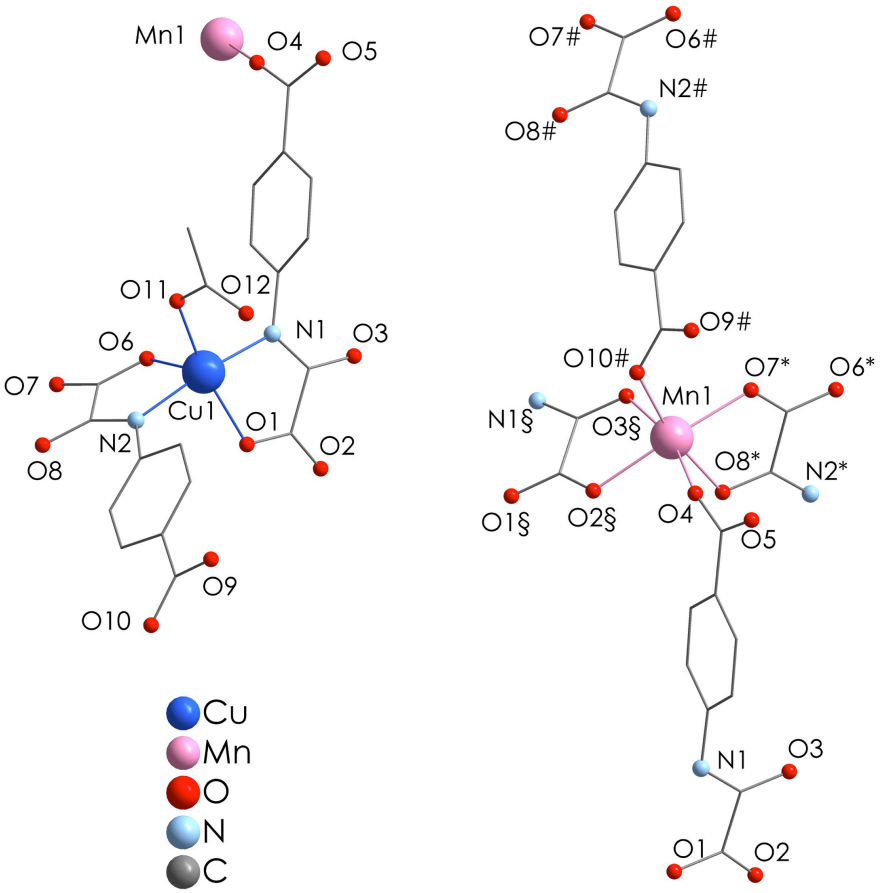


Figure 1. Representation of the coordination environments of the Cu(II) and Mn(II) ions together with selected atom labels (#: x,y,-1+z; *: 1/2+x,1/2-y,-1/2+z; §:-1/2+x,1/2-y,-1/2+z). H atoms are omitted for clarity.

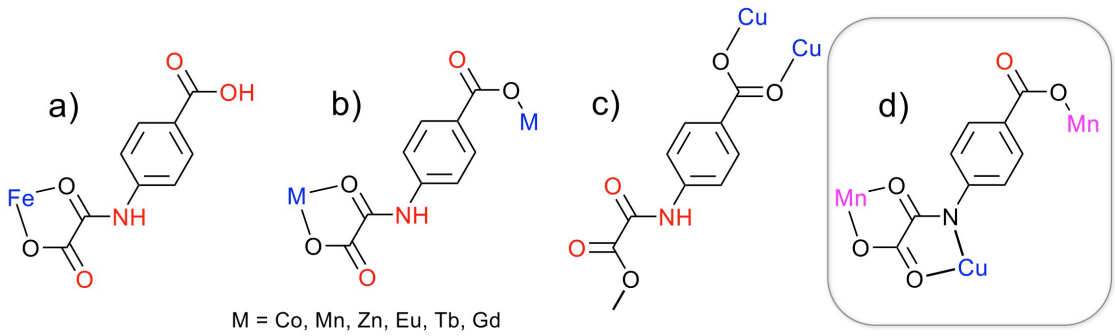


Scheme 1. Drawings of the known coordination mode for the {paba} ligand. a) ref.[27]; b) ref.[26–28]; c) ref.[26]; d) this work.

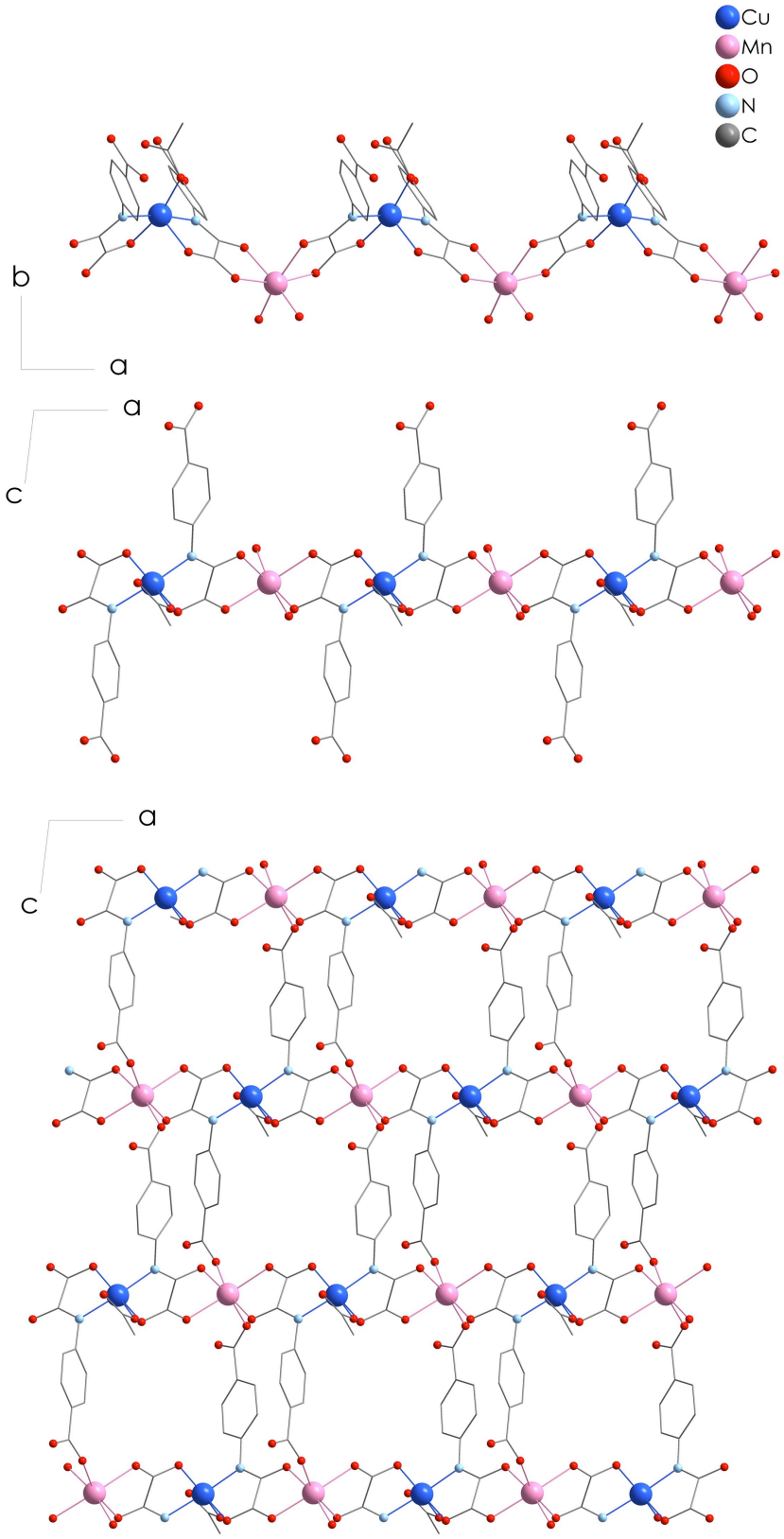


Figure 2. Representation of the {CuMn} zig-zag chain (top) with its pendent carboxylato groups aligned along *c* (middle). Bottom: view of the 2D brick-wall structure of **1** in the crystallographic (*ac*) plane. H atoms, $(TMA)^+$ counter-cations and solvent molecules are omitted for clarity.

In comparison to previously reported 2D brick-wall structures obtained with oxamate ligands, **1** shows one striking difference with its copper complex building unit.[42,43] Where bimetallic tetrakis-bidendate $\{Cu_2L_2\}$ metalloligands obtained from bis-oxamic ligands are traditionally used in bench conditions, here the monometallic $[Cu(paba)_2]^{4-}$ complex is –thanks to the additional coordinating groups born by the ligand– able to generate the same connectivity. As a consequence, the "rungs" and cavities of the brick-wall structure differ. In the previous oxamate-based 2D brick-wall architectures, the bimetallic metalloligand acted as the rung, and decametallic cavities were observed (Figure 3). In **1**, two half-complexes act as links between the 1D zig-zag chains and smaller tetrametallic cavities are obtained. The alternating pendent carboxylato groups, instead of the alternating metalloligands, actually give rise to a higher cross-linking of the chains.

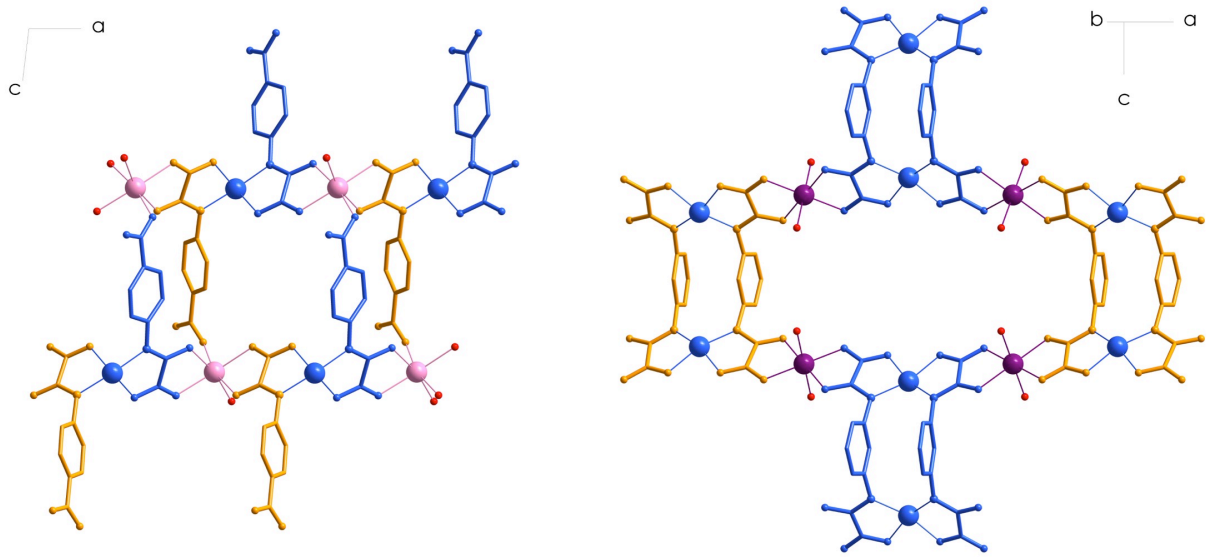


Figure 3. Comparison of the brick-wall arrangements in 1 (left) and in $[Co_2Cu_2(mpba)_2(H_2O)_6]$ (right).[42] H atoms, $(TMA)^+$ counter-cations, acetate groups and solvent molecules are omitted for clarity.

In the crystal lattice, the corrugated 2D layers are stacked parallel to each other in an eclipse fashion along the crystallographic *b* axis, with $TMA^+$ cations located between the planes (See Supporting Information). The shortest metal–metal interlayer separation is of 11.288(2) Å (Cu—Mn). Inter- and intra-layer hydrogen bonds are also present between crystallization water molecules and the uncoordinated oxygen atoms of the phenyl carboxylato groups and of the acetato groups (O---O distances ranging from 2.68 to 2.79 Å) (Figure S3).

In order to analyze the thermal stability of compound **1**, thermogravimetric analysis (TGA) and thermodiffraction measurements have been performed. TGA under air shows a two steps weight loss of 14.7 % between room temperature and 90 °C that corresponds to the water solvent molecules (ca. 15 %, see FigureS4 in the Supporting Information). It is followed by a plateau up to 200-210 °C before a sharp 70 % weight loss that should correspond to the organic content (*ca.* 74%). Indeed, TGA of the ligand alone shows decomposition between 200 and 250 °C. At 800 °C under air, the final weight percentage of 17 % matches well the calculated one for the formation of stoichiometric amounts of CuO and $Mn_2O_3$ (16.8 %). Temperature-dependent powder X-Ray diffraction measurements have been performed on **1**, under nitrogen and between room temperature and 600 °C (Figure 4). This investigation shows that the structure of compound **1** remains stable up to 90 °C. At this temperature, both peak shifts and peak appearances/disappearances indicate a phase transition. The formed phase, **1b**, is then stable up to 200 °C. Peaks intensities start to drop at 210 °C and the structure collapses at 230 °C. At higher temperature (> 240°C), the formation of oxides begins and is observed with the appearance of the corresponding diffraction peaks (CuO and $CuMn_2O$).

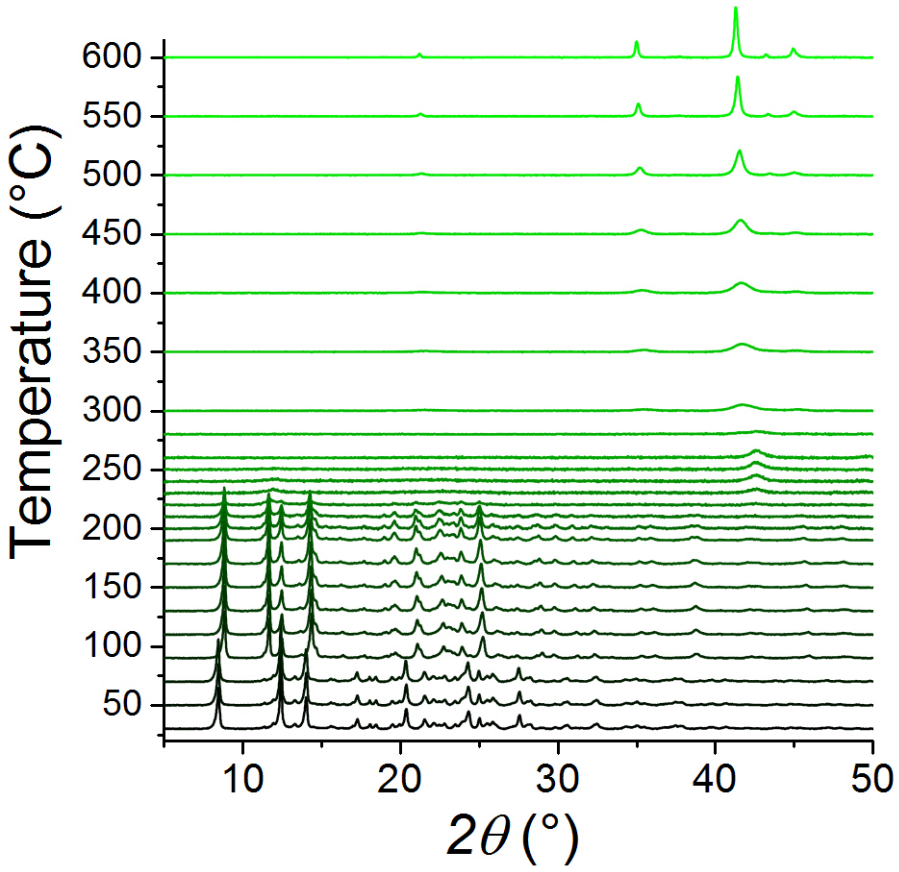


Figure 4. Thermodiffractograms of compound 1 from 30 °C to 600 °C under nitrogen.

To investigate the phase transition observed in the powder thermodiffraction measurements, we have collected the single crystal X-ray diffraction data on a sample that was heated at 5 °C/min to 92°C under the nitrogen stream of the diffractometer. It has revealed that the obtained phase belongs to the same space group than **1**, and is the dehydrated form of the 2D network, $(TMA)_3[CuMn(paba)_2(OAc)]$ (**1b**). The water removal leads to a moderate unit cell shrinkage, the initial volume of 4096 $Å^3$ decreases to 3772 $Å^3$. Within the 2D layer, the corrugated shape is accentuated, with a Mn–Cu–Mn angle decreased by 7°. In the lattice, shorter metal-metal interlayer distances are observed (Cu---Mn: 9.70(1) Å) and the packing of the layers is closer to an eclipsed arrangement (Figure 5). The structure of **1b** also presents several conformational differences with **1** that reflects the densification of the packing. The dihedral angles between the phenyl rings and the planes described by the oxamato groups in the ligands decrease in **1b**, going from 88° and 30° to 60° and 16° (Figure S7). There is also a decrease of the dihedral angle between the two phenyl rings in the asymmetric unit (from 71 to 58°). However, the dihedral angle between the two planes of the oxamato groups in the $[Cu(paba)_2]^{4-}$ building unit does not vary much (86 to 88°). Using caution since the low resolution of the X-Ray data for **1b** (1.19 Å) limits the comparison, there seem to be no significant differences in bonds lengths or angles in the coordination spheres of the metal ions between **1** and **1b**. The Mn(II) coordination sphere only seems slightly more distorted. Cu—O/$N_{eq}$ distances vary from 1.96(2) to 2.04(2) Å, with an apical Cu—O distance of 2.18(1) Å ; Mn—O distances average at 2.20 Å. It would therefore appear that the contraction of the packing is facilitated by the rotational degree of freedom around the nitrogen atom of the oxamato group.

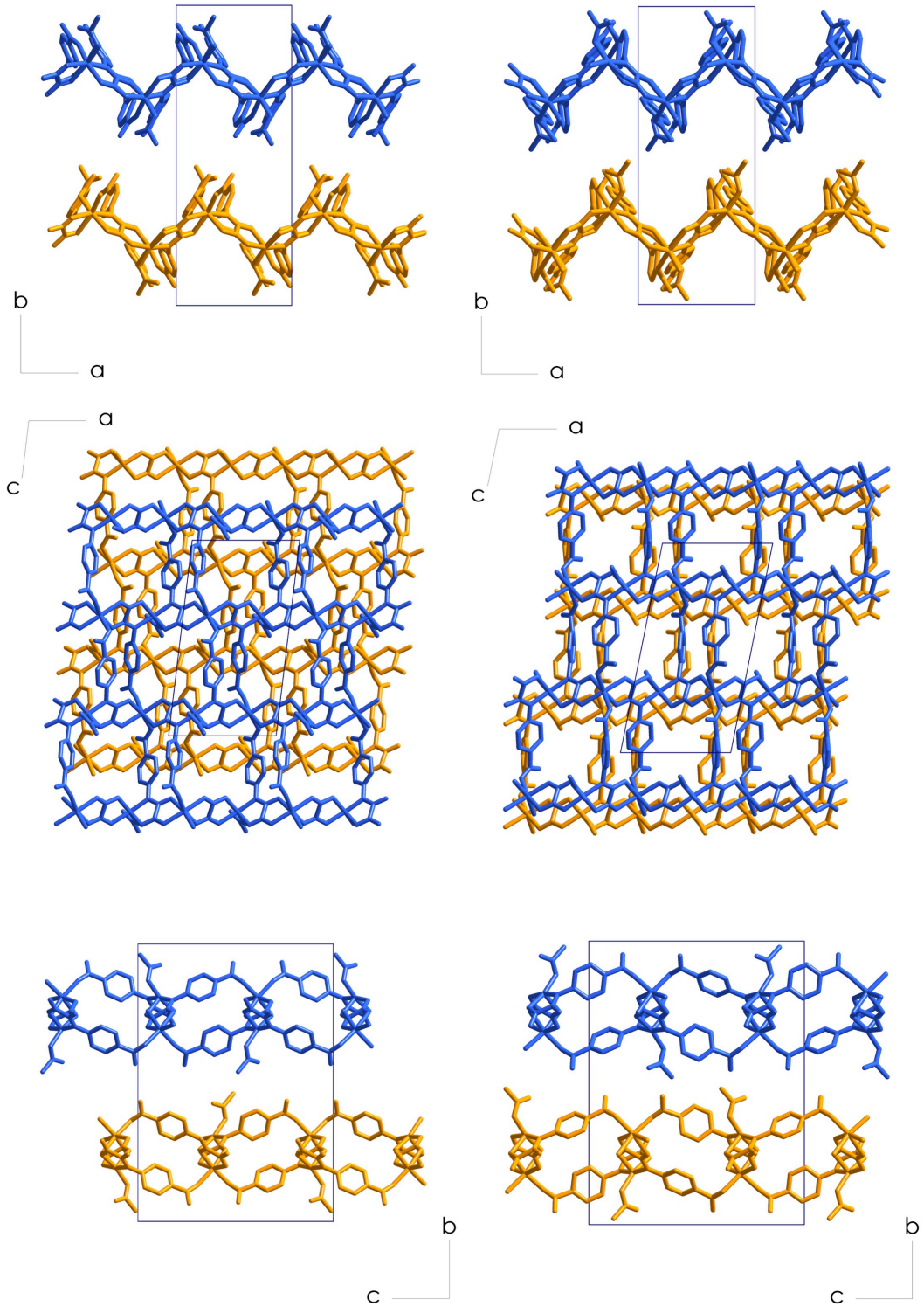


Figure 5. Comparison of the crystal packing in 1 (left) and 1b (right).

The dc magnetic property of compounds **1** and **1b** under an applied field of 2500 Oe in the form of $\chi_M T$ versus T plots are shown in Figure 6. The value of $\chi_M T$ for **1** and **1b** at room temperature are equal to 4.5 and 4.3 $cm^3$ K $mol^{-1}$ respectively. These values are slightly lower than the expected value for non-interacting Cu(II) and Mn(II) ions (4.78 $cm^3$ K $mol^{-1}$). Upon cooling, both $\chi_M T$ products decrease slowly down to 58 and 66 K and reach minima of 4.0 $cm^3$ K $mol^{-1}$ and 3.8 $cm^3$ K $mol^{-1}$, for **1** and **1b** respectively. Upon further cooling, the $\chi_M T$ products increase, following an expected ferrimagnetic behavior. They reach maxima of 14.4 and 17.3 $cm^3$ K $mol^{-1}$ at 4 and 4.5 K, for **1** and **1b** respectively, before decreasing to 9.8 and 11.9 $cm^3$ K $mol^{-1}$ at 2 K.

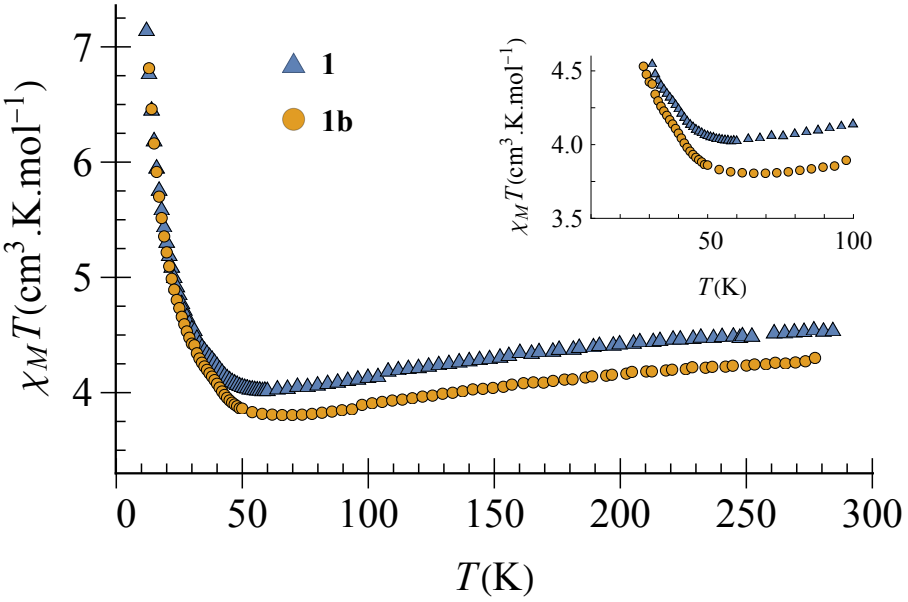


Figure 6. temperature dependence of the $c_M T$ product of compounds 1 (blue) and 1b (orange). Inset: $c_M T$ plots between 100 and 25 K.

A closer look at the curves' minimum region clearly shows an anomaly around 40 K (Figure S8). Under a lower field (100 Oe), this anomaly becomes more visible (Figure S8). The presence of a bump, the intensity of which decreases when increasing the magnetic field, signals the presence of a saturated ferromagnetic impurity. The ordering temperature near 40 K points to a $Mn_3O_4$ impurity, which displays magnetic ordering at 43 K.[44–46] Under a 100 Oe applied field, the $c_M T$ products abruptly increase between 8 and 2 K, reaching values of 49.4 $cm^3$ K $mol^{-1}$ for the hydrated phase **1**, and 99.4 $cm^3$ K $mol^{-1}$ for **1b** (see Figure S9). This sudden rise of $c_M T$ is a precursor sign of a magnetic ordering. The existence of a magnetic ordering is confirmed by the ZFC/FC curves for **1** (Figure 7). They diverge at 2.8 K, showing a magnetic ordering toward a ferrimagnetic phase at this temperature. The AC magnetic measurement for **1** (Figure 7) shows a frequency-independent maximum of $\chi_M''$ at 2.5 K, supporting the existence of the magnetic ordering observed in the ZFC/FC curves. The origin of the feature around 3.75 K is unclear and has no equivalent in the DC measurements.

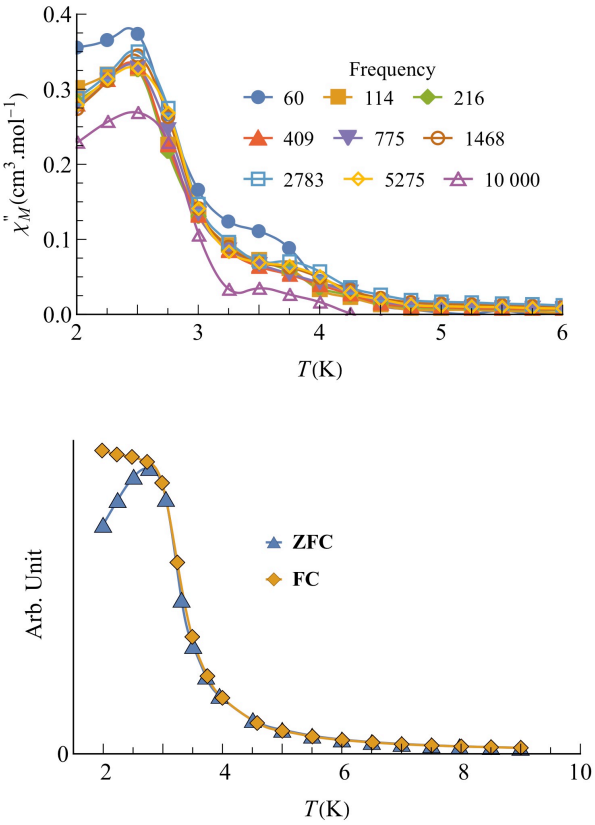


Figure 7. The $c_M''$ v. $T$ plot for compound 1 from 60 to 10000 Hz (top), and the ZFC/FC curves for 1 under a 100 Oe magnetic field (bottom). Solid lines are guide for the eye.

Field dependence of the magnetization was also investigated at 2 K for the two compounds (Figure 8). The curves are typical of compounds with a ferro- or ferri-magnetic order, i.e. a magnetization that rapidly increases at low magnetic field values. The ferrimagnetic nature of the ordering is indicated by the saturation magnetization values of 3.30 and 3.55 *Nb* reached at 7 T by **1** and **1b** respectively. These values are closed to the expected one for an antiferromagnetically coupled {CuMn} metal ions pair ($S$ = 2). Compounds **1** and **1b** do not show hysteresis loops (Figure S10). They contain only Cu(II) and Mn(II) ions, which are not very anisotropic ions.

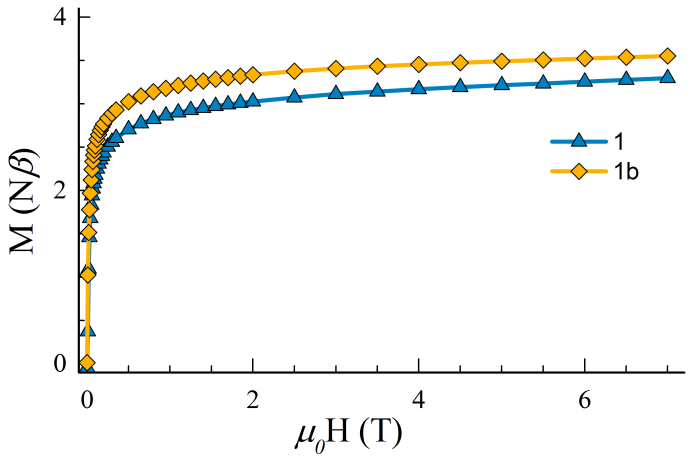


Figure 8. Magnetization versus field for compounds 1 and 1b measured at 2 K. Solid lines are guide for the eye.

It is well established that the interaction between a Cu(II) ion and a Mn(II) ion through an oxamato bridge is antiferromagnetic.[47,48] This leads, along the {CuMn} oxamato chain, to an alternation of

positive and negative spin densities on the metal ion centers. On the other hand, the interaction between the Cu(II) and Mn(II) ions through the phenylcarboxylato bridge is not known. However, the appearance of a ferrimagnetic type of magnetic order shows that this interaction is antiferromagnetic with a mechanism reminiscent to that of McConnell for organic radicals.[49] A positive spin density interacts antiferromagnetically with the negative spin density of its nearest neighbor, as illustrated in Figure 9. A ferromagnetic coupling between the Cu(II) and Mn(II) ions through the phenylcarboxylato bridge would lead to an effective antiferromagnetic coupling between the {CuMn} oxamato chains and the magnetic moment of a chain being annihilated by its neighbor (see Figure S11 in the Supporting information).

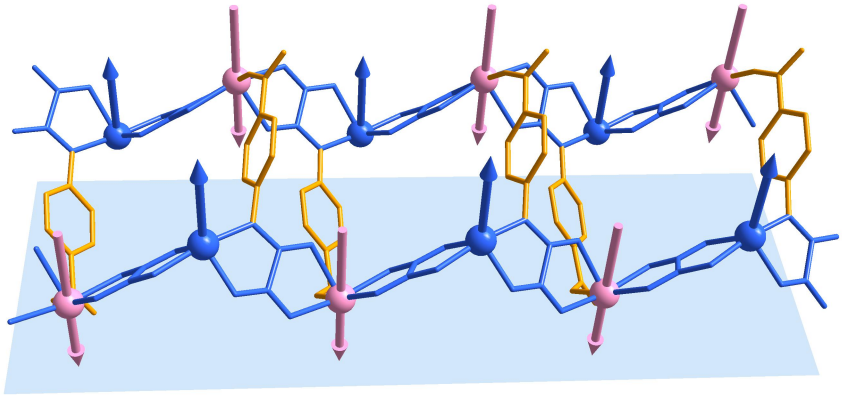

Figure 9. Effective McConnell-type ferromagnetic coupling between two adjecnt chains by antiferromagnetic interaction between spin densities of opposite directions on neighboring chains.

As stated above, the Cu(II) and Mn(II) ions are not anisotropic and the ferrimagnetic plane is of Heisenberg type. It cannot lead to a magnetic ordering in 2D. To obtain a magnetic order, ferromagnetic interplane interactions are compulsory. This interaction is weak, whether it is dipolar in origin or a McConnell type effective interplanar ferromagnetic interaction arising from the H-bonds network (Figure S3). This explains the very low critical temperature of 2.5 K measured for compound **1**. Interplanar antiferromagnetic interactions would lead to a metamagnetic behavior that was not observed.

## CONCLUSION.

An oxamate-based 2D heterobimetallic compound was synthesized solvothermally. Its structure is that of a brick-wall arrangement, bearing differences with previously reported corrugated oxamato-bridged 2D open-framework. The use here of a multi-polydentate oxamate ligand with the presence of the additional carboxylato coordinating group has allowed the construction of the 2D structure from monometallic bis-oxamato complexes, instead of the bimetallic tetrakis-oxamato metalloligands traditionally used. Temperature dependent X-ray diffraction has revealed that the compound can withstand desolvation and retain its crystallinity up to 200 °C. Magnetic measurements have indicated the formation of a ferrimagnetic compound showing a critical temperature of 2.8 K resulting from both intra-layer antiferromagnetic interactions and inter-layer ferromagnetic interaction. Unfortunately, low field measurements have also revealed traces of a manganese oxide impurity, probably inherent to the synthetic conditions. Nevertheless, the isolation of **1** clearly supports the development of solvothermal synthesis, particularly to react more complex forms of oxamate ligands and prepare ferrimagnetic compounds.

## ACKNOWLEDGMENT

This work was supported by the Ministère de l'Enseignement Supérieur, de la Recherche et de l'Innovation (MESRI), the Centre National de la Recherche Scientifique (CNRS) and the China Scholarship Council (CSC) with M. Ang Li's PhD fellowship. Elemental analysis was supported by the IPGP multidisciplinary program PARI, and by Paris–IdF region SESAME Grant no. 12015908. We acknowledge SOLEIL for provision of synchrotron radiation facilities at the CRISTAL beamline (BAG Proposal 20170946). We thank the French network RECIPROCS and P. Fertey for his help. We thank the staff of the low temperature physical measurement MPBT technical platform in Sorbonne Université.

## REFERENCES

(1) Grancha, T.; Ferrando-Soria, J.; Castellano, M.; Julve, M.; Pasán, J.; Armentano, D.; Pardo, E. Oxamato-Based Coordination Polymers: Recent Advances in Multifunctional Magnetic Materials. *Chem. Commun.* **2014**, *50* (57), 7569–7585. https://doi.org/10.1039/C4CC01734J.

(2) Mon, M.; Bruno, R.; Ferrando-Soria, J.; Armentano, D.; Pardo, E. Metal–Organic Framework Technologies for Water Remediation: Towards a Sustainable Ecosystem. *J. Mater. Chem. A* **2018**, *6* (12), 4912–4947. https://doi.org/10.1039/C8TA00264A.

(3) Viciano-Chumillas, M.; Mon, M.; Ferrando-Soria, J.; Corma, A.; Leyva-Pérez, A.; Armentano, D.; Pardo, E. Metal–Organic Frameworks as Chemical Nanoreactors: Synthesis and Stabilization of Catalytically Active Metal Species in Confined Spaces. *Acc. Chem. Res.* **2020**, *53* (2), 520–531. https://doi.org/10.1021/acs.accounts.9b00609.

(4) Ruiz, R.; Faus, J.; Lloret, F.; Julve, M.; Journaux, Y. Coordination Chemistry of N,N′-Bis(Coordinating Group Substituted)Oxamides: A Rational Design of Nuclearity Tailored Polynuclear Complexes. *Coordination Chemistry Reviews* **1999**, *193–195*, 1069–1117. https://doi.org/10.1016/S0010-8545(99)00138-1.

(5) Pardo, E.; Ruiz-Garcia, R.; Cano, J.; Ottenwaelder, X.; Lescouëzec, R.; Journaux, Y.; Lloret, F.; Julve, Miguel. Ligand Design for Multidimensional Magnetic Materials: A Metallo-Supramolecular Perspective. *Dalton Trans.* **2008**, No. 21, 2780–2805. https://doi.org/10.1039/b801222a.

(6) Dul, M.-C.; Pardo, E.; Lescouëzec, R.; Journaux, Y.; Ferrando-Soria, J.; Ruiz-Garcia, R.; Cano, J.; Julve, M.; Lloret, F.; Cangussu, D.; Pereira, C. L. M.; Stumpf, H. O.; Pasan, J.; Ruiz-Perez, C. Supramolecular Coordination Chemistry of Aromatic Polyoxalamide Ligands: A Metallosupramolecular Approach toward Functional Magnetic Materials. *Coord. Chem. Rev.* **2010**, *254* (19–20), 2281–2296. https://doi.org/10.1016/j.ccr.2010.03.003.

(7) Journaux, Y.; Ferrando-Soria, J.; Pardo, E.; Ruiz-Garcia, R.; Julve, M.; Lloret, F.; Cano, J.; Li, Y.; Lisnard, L.; Yu, P.; Stumpf, H.; Pereira, C. L. M. Design of Magnetic Coordination Polymers Built from Polyoxalamide Ligands: A Thirty Year Story. *Eur. J. Inorg. Chem.* **2018**, *2018* (3–4), 228–247. https://doi.org/10.1002/ejic.201700984.

(8) Pardo, E.; Burguete, P.; Ruiz-Garc?a, R.; Julve, M.; Beltr?n, D.; Journaux, Y.; Amor?s, P.; Lloret, F. Ordered Mesoporous Silicas as Host for the Incorporation and Aggregation of Octanuclear Nickel(Ii) Single-Molecule Magnets: A Bottom-up Approach to New Magnetic Nanocomposite Materials. *J. Mater. Chem.* **2006**, *16* (26), 2702. https://doi.org/10.1039/b602838a.

(9) Castellano, M.; Ruiz-García, R.; Cano, J.; Ferrando-Soria, J.; Pardo, E.; Fortea-Pérez, F. R.; Stiriba, S.-E.; Barros, W. P.; Stumpf, H. O.; Cañadillas-Delgado, L.; Pasán, J.; Ruiz-Pérez, C.; de Munno, G.; Armentano, D.; Journaux, Y.; Lloret, F.; Julve, M. Metallosupramolecular Approach toward Multifunctional Magnetic Devices for Molecular Spintronics. *Coord. Chem. Rev.* **2015**, *303*, 110–138. https://doi.org/10.1016/j.ccr.2015.05.013.

(10) Pardo, E.; Ruiz-Garcia, R.; Lloret, F.; Faus, J.; Julve, M.; Journaux, Y.; Delgado, F.; Ruiz-Perez, Catalina. Cobalt(II)-Copper(II) Bimetallic Chains as a New Class of Single-Chain Magnets. *Adv. Mater.* **2004**, *16* (18), 1597–1600. https://doi.org/10.1002/adma.200400253.

(11) Pei, Yu.; Verdaguer, Michel.; Kahn, Olivier.; Sletten, Jorunn.; Renard, J. Pierre. Ferromagnetic Transition in a Bimetallic Molecular System. *J. Am. Chem. Soc.* **1986**, *108* (23), 7428–7430. https://doi.org/10.1021/ja00283a059.

(12) Nakatani, Keitaro.; Bergerat, Pierre.; Codjovi, Epiphane.; Mathoniere, Corine.; Pei, Yu.; Kahn, Olivier. Optimization of a Molecular-Based [Manganese Copper] Magnet: MnCu(PbaOH)(H2O)2 (PbaOH = 2-Hydroxy-1,3-Propylenebis(Oxamato)) with Tc = 30 K. *Inorganic Chemistry* **1991**, *30* (21), 3977–3978. https://doi.org/10.1021/ic00021a001.

(13) Stumpf, H. O.; Pei, Y.; Kahn, O.; Ouahab, L.; Grandjean, D. A Molecular-Based Magnet with a Fully Interlocked Three-Dimensional Structure. *Science* **1993**, *261* (5120), 447–449. https://doi.org/10.1126/science.261.5120.447.

(14) Pardo, E.; Cangussu, D.; Dul, M.-C.; Lescouëzec, R.; Herson, P.; Journaux, Y.; Pedroso, E. F.; Pereira, C. L. M.; Muñoz, M. C.; Ruiz-García, R.; Cano, J.; Amorós, P.; Julve, M.; Lloret, F. A Metallacryptand-Based Manganese(II)–Cobalt(II) Ferrimagnet with a Three-Dimensional Honeycomb Open-Framework Architecture. *Angew. Chem., Int. Ed.* **2008**, *47* (22), 4211–4216. https://doi.org/10.1002/anie.200800208.

(15) Ferrando-Soria, J.; Ruiz-Garcia, R.; Cano, J.; Stiriba, S.-E.; Vallejo, J.; Castro, I.; Julve, M.; Lloret, F.; Amoros, P.; Pasan, J.; Ruiz-Perez, C.; Journaux, Y.; Pardo, Emilio. Reversible Solvatomagnetic Switching in a Spongelike Manganese(II)-Copper(II) 3D Open Framework with a Pillared Square/Octagonal Layer Architecture. *Chem.--Eur. J.* **2012**, *18* (6), 1608–1617. https://doi.org/10.1002/chem.201103308.

(16) Grancha, T.; Ferrando-Soria, J.; Zhou, H.-C.; Gascon, J.; Seoane, B.; Pasán, J.; Fabelo, O.; Julve, M.; Pardo, E. Postsynthetic Improvement of the Physical Properties in a Metal–Organic Framework through a Single Crystal to Single Crystal Transmetallation. *Angew. Chem. Int. Ed.* **2015**, *54* (22), 6521–6525. https://doi.org/10.1002/anie.201501691.

(17) Abhervé, A.; Grancha, T.; Ferrando-Soria, J.; Clemente-León, M.; Coronado, E.; Waerenborgh, J. C.; Lloret, F.; Pardo, E. Spin-Crossover Complex Encapsulation within a Magnetic Metal–Organic Framework. *Chem. Commun.* **2016**, *52* (46), 7360–7363. https://doi.org/10.1039/C6CC03667H.

(18) Mon, M.; Bruno, R.; Sanz-Navarro, S.; Negro, C.; Ferrando-Soria, J.; Bartella, L.; Di Donna, L.; Prejanò, M.; Marino, T.; Leyva-Pérez, A.; Armentano, D.; Pardo, E. Hydrolase–like Catalysis and Structural Resolution of Natural Products by a Metal–Organic Framework. *Nature Communications* **2020**, *11* (1), 3080. https://doi.org/10.1038/s41467-020-16699-3.

(19) Bruno, R.; Mon, M.; Escamilla, P.; Ferrando-Soria, J.; Esposito, E.; Fuoco, A.; Monteleone, M.; Jansen, J. C.; Elliani, R.; Tagarelli, A.; Armentano, D.; Pardo, E. Bioinspired Metal-Organic Frameworks in Mixed Matrix Membranes for Efficient Static/Dynamic Removal of Mercury from Water. *Advanced Functional Materials* **2021**, *31* (6), 2008499. https://doi.org/10.1002/adfm.202008499.

(20) Negro, C.; Martínez Pérez-Cejuela, H.; Simó-Alfonso, E. F.; Herrero-Martínez, J. M.; Bruno, R.; Armentano, D.; Ferrando-Soria, J.; Pardo, E. Highly Efficient Removal of Neonicotinoid Insecticides by Thioether-Based (Multivariate) Metal–Organic Frameworks. *ACS Appl. Mater. Interfaces* **2021**, *13* (24), 28424–28432. https://doi.org/10.1021/acsami.1c08833.

(21) Tursi, A.; Mastropietro, T. F.; Bruno, R.; Baratta, M.; Ferrando-Soria, J.; Mashin, A. I.; Nicoletta, F. P.; Pardo, E.; De Filpo, G.; Armentano, D. Synthesis and Enhanced Capture Properties of a New BioMOF@SWCNT-BP: Recovery of the Endangered Rare-Earth Elements from Aqueous Systems. *Advanced Materials Interfaces* **2021**, *8* (16), 2100730. https://doi.org/10.1002/admi.202100730.

(22) da Cunha, T. T.; Barbosa, V. M. M.; Oliveira, W. X. C.; Pinheiro, C. B.; Pedroso, E. F.; Nunes, W. C.; Pereira, C. L. M. Slow Magnetic Relaxation in Mononuclear Gadolinium(III) and Dysprosium(III) Oxamato Complexes. *Polyhedron* **2019**, *169*, 102–113. https://doi.org/10.1016/j.poly.2019.04.056.

(23) da Cunha, T. T.; Barbosa, V. M. M.; Oliveira, W. X. C.; Pedroso, E. F.; García, D. M. A.; Nunes, W. C.; Pereira, C. L. M. Field-Induced Slow Magnetic Relaxation of a Six-Coordinate Mononuclear Manganese(II) and Cobalt(II) Oxamate Complexes. *Inorg. Chem.* **2020**, *59* (18), 12983–12987. https://doi.org/10.1021/acs.inorgchem.0c01628.

(24) Cunha, T. T. da; Silveira, C. O. C. da; Barbosa, V. M. M.; Oliveira, W. X. C.; Júnior, E. N. da S.; Ferreira, F. F.; Pedroso, E. F.; Pereira, C. L. M. Ferromagnetic Coupling in a Dicopper(II) Oxamate Complex Bridged by Carboxylate Groups. *CrystEngComm* **2021**. https://doi.org/10.1039/D0CE01742F.

(25) Yoneda, K.; Hori, Y.; Ohba, M.; Kitagawa, S. A Homometallic Ferrimagnet Based on Mixed Antiferromagnetic and Ferromagnetic Interactions through Oxamato and Carboxylato Bridges. *Chem. Lett.* **2008**, *37* (1), 64–65. https://doi.org/10.1246/cl.2008.64.

(26) Oliveira, T. L.; Kalinke, L. H. G.; Mascarenhas, E. J.; Castro, R.; Martins, F. T.; Sabino, J. R.; Stumpf, H. O.; Ferrando, J.; Julve, M.; Lloret, F.; Cangussu, D. Cobalt(II) and Copper(II) Assembling through a Functionalized Oxamate-Type Ligand. *Polyhedron* **2014**, *81*, 105–114. https://doi.org/10.1016/j.poly.2014.05.051.

(27) Maciel, J.; Kalinke, L.; Valdo, A.; Martins, F.; Rabelo, R.; Moliner, N.; Cano, J.; Julve, M.; Lloret, F.; Cangussu, D. New Metal-Organic Systems with a Functionalized Oxamate-Type Ligand and MnII, FeII, CuII and ZnII. *J. Braz. Chem. Soc.* **2019**, *30* (11), 2413–2429. https://doi.org/10.21577/0103-5053.20190158.

(28) de Oliveira Maciel, J. W.; Lemes, M. A.; Valdo, A. K.; Rabelo, R.; Martins, F. T.; Queiroz Maia, L. J.; de Santana, R. C.; Lloret, F.; Julve, M.; Cangussu, D. Europium(III), Terbium(III), and Gadolinium(III) Oxamato-Based Coordination Polymers: Visible Luminescence and Slow Magnetic Relaxation. *Inorg. Chem.* **2021**. https://doi.org/10.1021/acs.inorgchem.0c03226.

(29) Li, A.; Li, Y.; Chamoreau, L.-M.; Desmarets, C.; Lisnard, L.; Journaux, Y. A Bis-Polydentate Oxamate-Based Achiral Ligand That Can Stabilize a Macrocyclic Mixed Valence Compound or Induce a 1D Helical Chain. *Eur. J. Inorg. Chem.* **2020**, *2020* (34), 3311–3319. https://doi.org/10.1002/ejic.202000490.

(30) Li, A.; Chamoreau, L.-M.; Baptiste, B.; Li, Y.; Journaux, Y.; Lisnard, L. Solvothermal Synthesis, Structure and Magnetic Properties of Heterometallic Coordination Polymers Based on a Phenolato-Oxamato Co-Bidentate-Tridentate Ligand. *Dalton Trans.* **2021**, *50* (2), 681–688. https://doi.org/10.1039/D0DT03269G.

(31) Li, A.; Forté, J.; Li, Y.; Journaux, Y.; Lisnard, L. Synthesis, Structure and Magnetic Properties of an Oxamate-Based 1D Coordination Polymer Built on Pentametallic Links. *Inorg. Chim. Acta* **2021**, *521*, 120320. https://doi.org/10.1016/j.ica.2021.120320.

(32) Cervera, B.; Sanz, J. L.; Ibáñez, M. J.; Vila, G.; LLoret, F.; Julve, M.; Ruiz, R.; Ottenwaelder, X.; Aukauloo, A.; Poussereau, S.; Journaux, Y.; Munoz, M. C. Stabilization of Copper (III) Complexes by Substituted Oxamate Ligands. *J. Chem. Soc., Dalton Trans.* **1998**, No. 5, 781–790. https://doi.org/10.1039/A706964B.

(33) *CrysAlisPro CCD and CrisAlisPro RED*, Oxford Diffraction Ltd., Yarnton, Oxfordshire, U.K.; 2009.

(34) Blessing, R. H. *Crystallogr. Rev.* **1987**, *1*, 3.

(35) Blessing, R. H. An Empirical Correction for Absorption Anisotropy. *Acta Cryst A* **1995**, *51*, 33. https://doi.org/10.1107/S0108767394005726.

(36) *BrukerAXS Inc*, Madison, Wisconsin, USA.; 1998.

(37) Sheldrick, G. M. SHELXT – Integrated Space-Group and Crystal-Structure Determination. *Acta Cryst A* **2015**, *71* (1), 3–8. https://doi.org/10.1107/S2053273314026370.

(38) Sheldrick, G. M. Crystal Structure Refinement with SHELXL. *Acta Crystallogr., Sect. C* **2015**, *71* (1), 3–8. https://doi.org/10.1107/S2053229614024218.

(39) Dolomanov, O. V.; Bourhis, L. J.; Gildea, R. J.; Howard, J. a. K.; Puschmann, H. OLEX2: A Complete Structure Solution, Refinement and Analysis Program. *J Appl Cryst* **2009**, *42* (2), 339–341. https://doi.org/10.1107/S0021889808042726.

(40) Rietveld, H. M. A Profile Refinement Method for Nuclear and Magnetic Structures. *J. Appl. Cryst.* **1969**, *2* (2), 65–71. https://doi.org/10.1107/S0021889869006558.

(41) Rodríguez-Carvajal, J. Recent Advances in Magnetic Structure Determination by Neutron Powder Diffraction. *Physica B: Condensed Matter* **1993**, *192* (1), 55–69. https://doi.org/10.1016/0921-4526(93)90108-I.

(42) Pereira, C. L. M.; Pedroso, E. F.; Stumpf, H. O.; Novak, M. A.; Ricard, L.; Ruiz-García, R.; Rivière, E.; Journaux, Y. A CuIICoII Metallacyclophane-Based Metamagnet with a Corrugated Brick-Wall Sheet Architecture. *Angew. Chem. Int. Ed. Engl.* **2004**, *43* (8), 956–958. https://doi.org/10.1002/anie.200352604.

(43) Ferrando-Soria, J.; Pasán, J.; Ruiz-Pérez, C.; Journaux, Y.; Julve, M.; Lloret, F.; Cano, J.; Pardo, E. Spin Control in Oxamato-Based Manganese(II)–Copper(II) Coordination Polymers with Brick-Wall Layer Architectures. *Inorg. Chem.* **2011**, *50* (18), 8694–8696. https://doi.org/10.1021/ic201437u.

(44) Boucher, B.; Buhl, R.; Perrin, M. Proprietes et Structure Magnetique de Mn3O4. *Journal of Physics and Chemistry of Solids* **1971**, *32* (10), 2429–2437. https://doi.org/10.1016/S0022-3697(71)80239-1.

(45) Nogues, M.; Poix, P. Contribution a l'etude Des Proprietes Ferrimagnetiques Du Systeme t. Mn3O4 + (1 – t). Mn2SnO4. *Solid State Communications* **1974**, *15* (3), 463–470. https://doi.org/10.1016/0038-1098(74)91121-1.

(46) Jensen, G. B.; Nielsen, O. V. The Magnetic Structure of Mn3O4Hausmannite between 4.7K and Neel Point, 41K. *J. Phys. C: Solid State Phys.* **1974**, *7* (2), 409–424. https://doi.org/10.1088/0022-3719/7/2/019.

(47) Pei, Yu.; Kahn, Olivier.; Sletten, Jorunn. Polymetallic Systems with Subtle Spin Orders. *J. Am. Chem. Soc.* **1986**, *108* (11), 3143–3145. https://doi.org/10.1021/ja00271a075.

(48) Pei, Y.; Journaux, Y.; Kahn, O.; Dei, A.; Gatteschi, D. A MnIICuIIMnII Trinuclear Species with an S= 9/2 Ground State. *J. Chem. Soc., Chem. Commun.* **1986**, No. 16, 1300–1301.

(49) McConnell, H. M. Ferromagnetism in Solid Free Radicals. *The Journal of Chemical Physics* **1963**, *39* (7), 1910–1910. https://doi.org/10.1063/1.1734562.

# Supporting information for:

## Solvothermal synthesis, temperature-dependent structural study and magnetic characterization of a multi-polydentate oxamate-based 2D coordination network.

*Ang Li,[#] Lise-Marie Chamoreau,[#] Benoît Baptiste,[§] Ludovic Delbes,[§] Yanling li,[#] Francesc Lloret,[‡] Yves Journaux,[#] and Laurent Lisnard[#]*.*

# Sorbonne Université, CNRS, Institut Parisien de Chimie Moléculaire, IPCM, F-75252, Paris, France.

§ Sorbonne Université, CNRS, IRD, MNHN, Institut de Minéralogie, de Physique des Matériaux et de Cosmochimie, IMPMC, F-75252, Paris, France

‡ Departament de Química Inorgànica/ Instituto de Ciencia Molecular (ICMol), Facultat de Química de la Universitat de València, València, Paterna, Spain 46980.

| Atoms | | dist. | Mn(II) | Mn(III) | Atoms | | dist. | Mn(II) | Mn(III) |
|---|---|---|---|---|---|---|---|---|---|
| Mn1 | O4 | 2.1142 | 0.416 | 0.384 | Mn1 | O4 | 2.0774 | 0.46 | 0.424 |
| | O10 | 2.1163 | 0.416 | 0.382 | | O7 | 2.1349 | 0.394 | 0.363 |
| | O7 | 2.1442 | 0.384 | 0.354 | | O10 | 2.166 | 0.362 | 0.334 |
| | O2 | 2.2009 | 0.329 | 0.304 | | O2 | 2.1976 | 0.332 | 0.306 |
| | O8 | 2.2056 | 0.325 | 0.3 | | O8 | 2.275 | 0.27 | 0.249 |
| | O3 | 2.2267 | 0.307 | 0.283 | | O3 | 2.3198 | 0.239 | 0.22 |
| | | | 2.176 | 2.007 | | | | 2.056 | 1.896 |

Table S1. BVS calculations for compound 1 and 1b.[1,2]

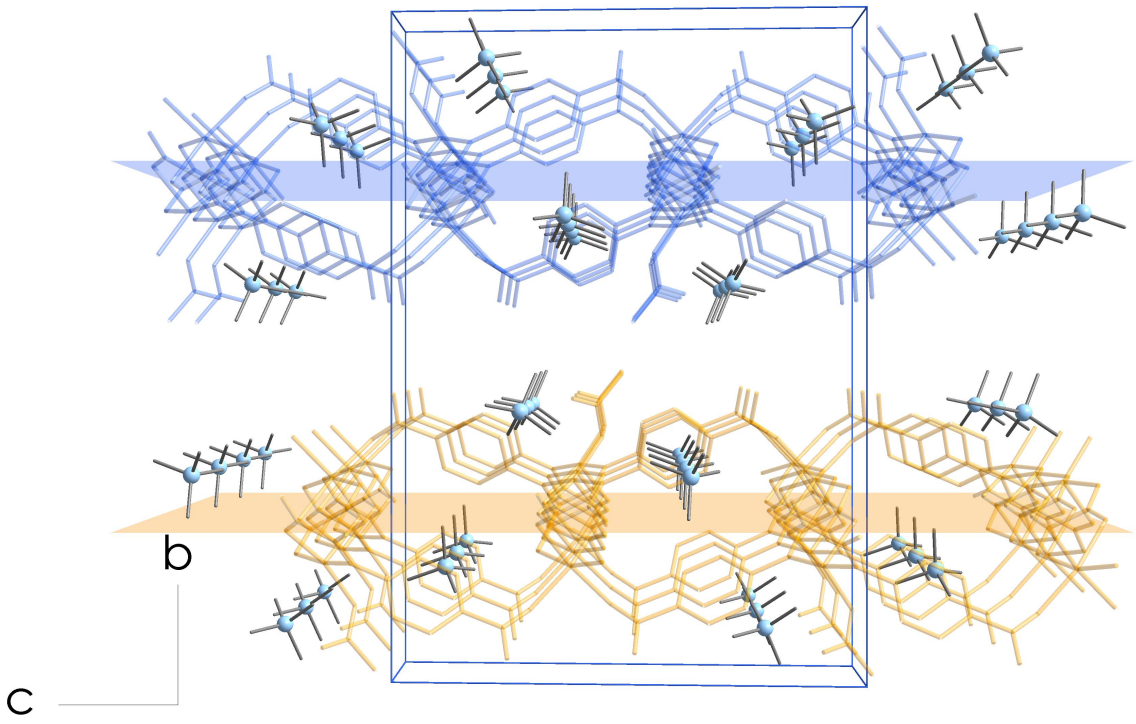


Figure S1. Representation of the $(TMA)^+$ cations in the crystal packing of 1, view along a.

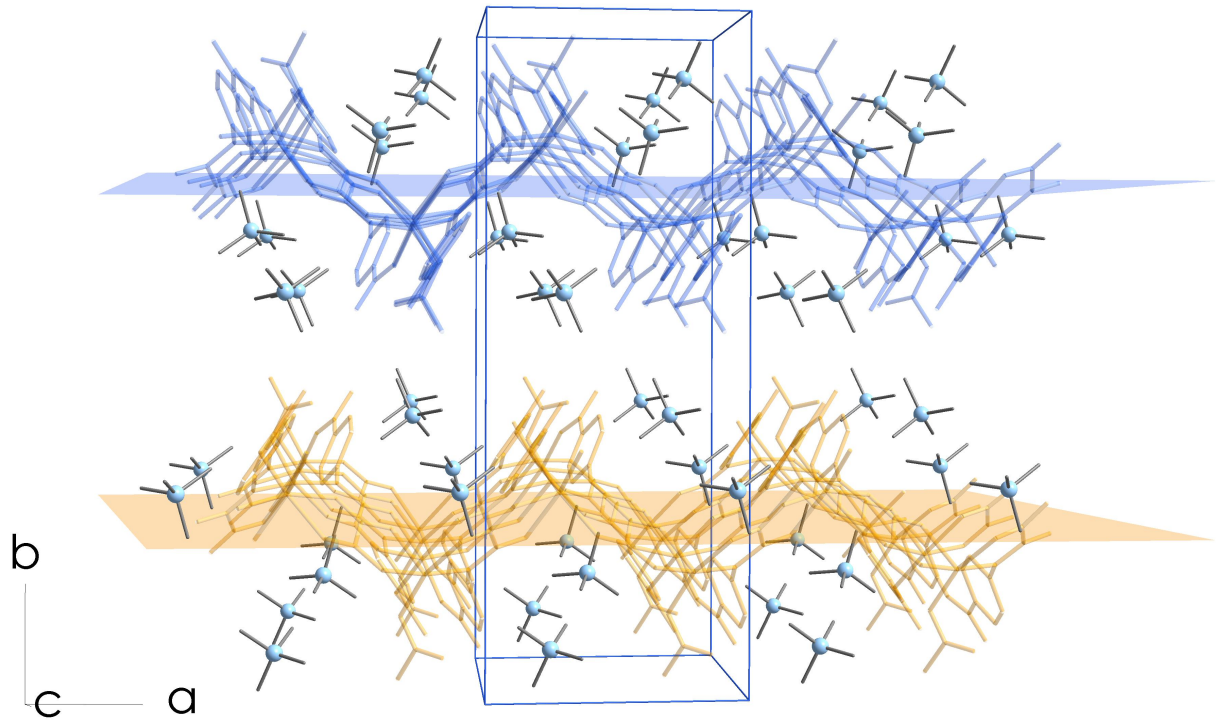


Figure S2. Representation of the $(TMA)^{+}$ cations in the crystal packing of 1, view along c.

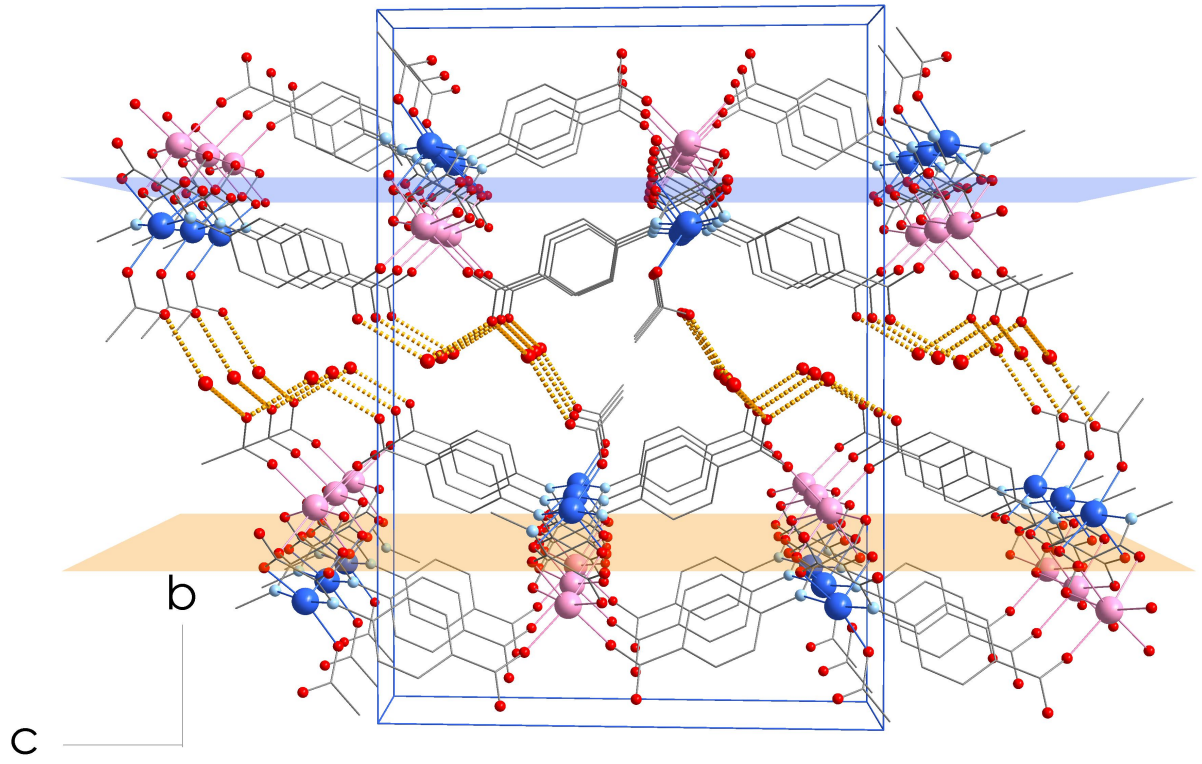


Figure S3. Representation of the H-bonds networking (orange doted lines) in the crystal packing of 1.

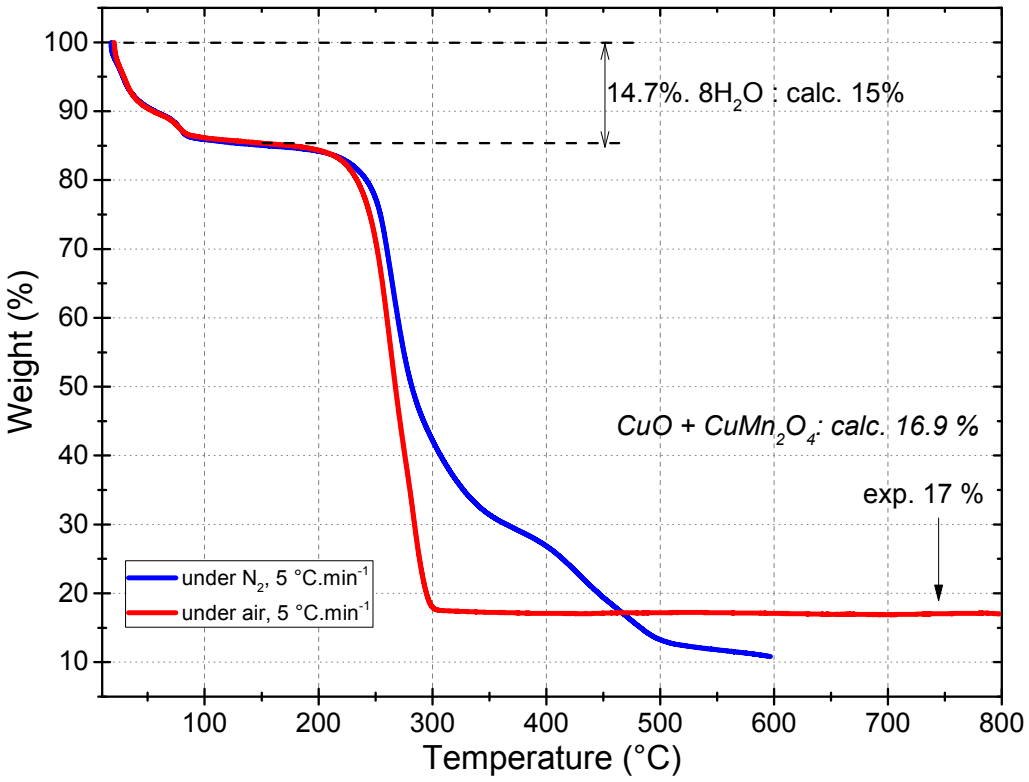


Figure S4. TGA of 1 performed under air or $N_2$.

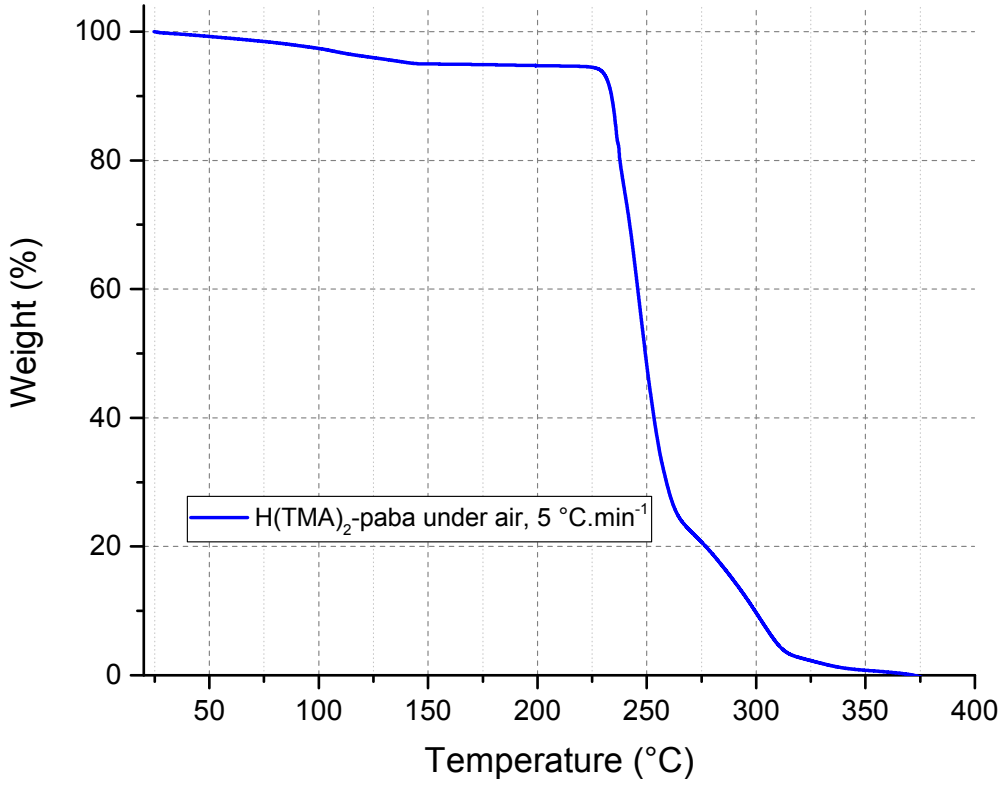


Figure S5. TGA under air of the ligand.

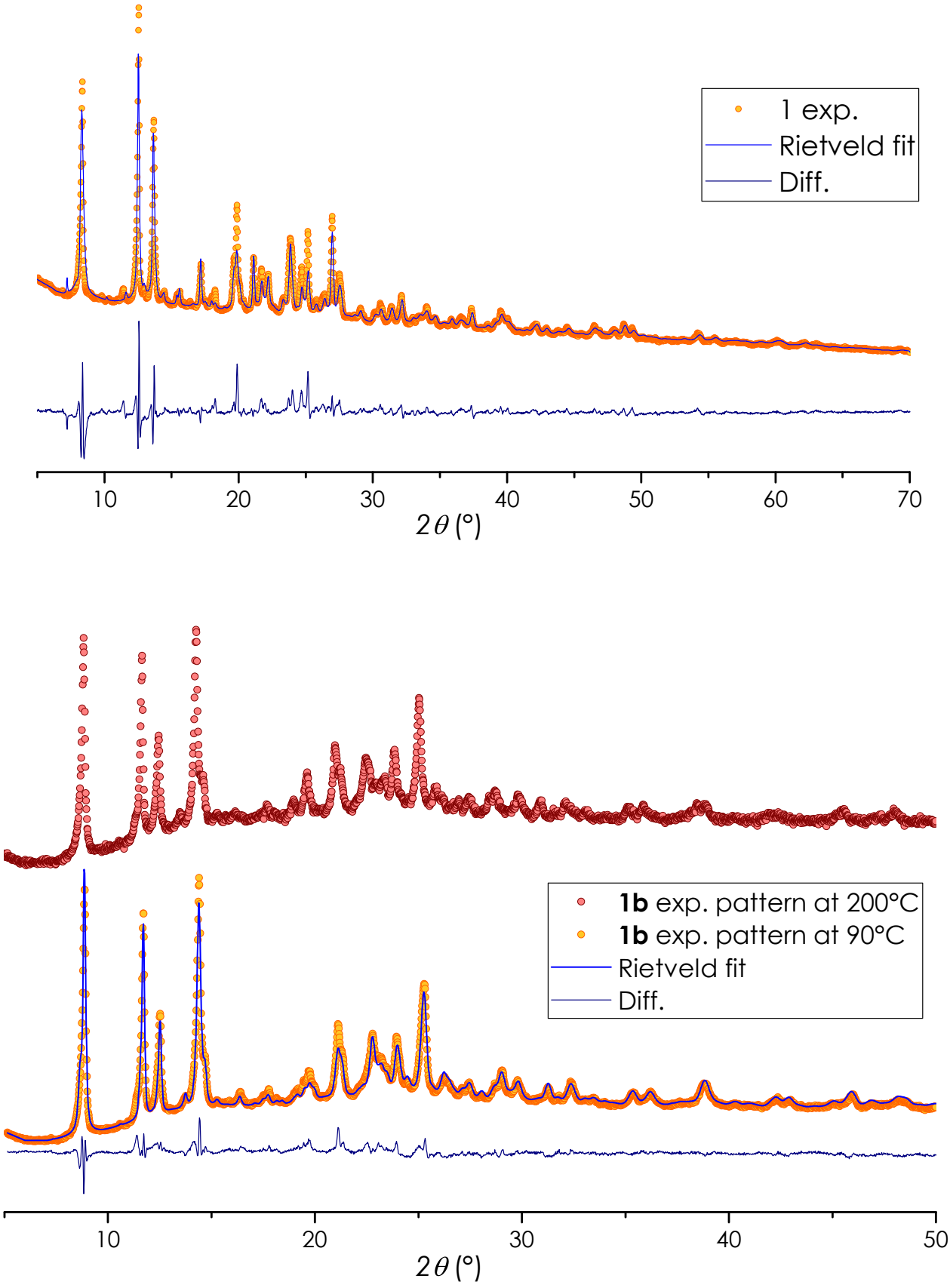


Figure S6. Experimental powder patterns and Rietveld refinements for 1 (top) and 1b (bottom).

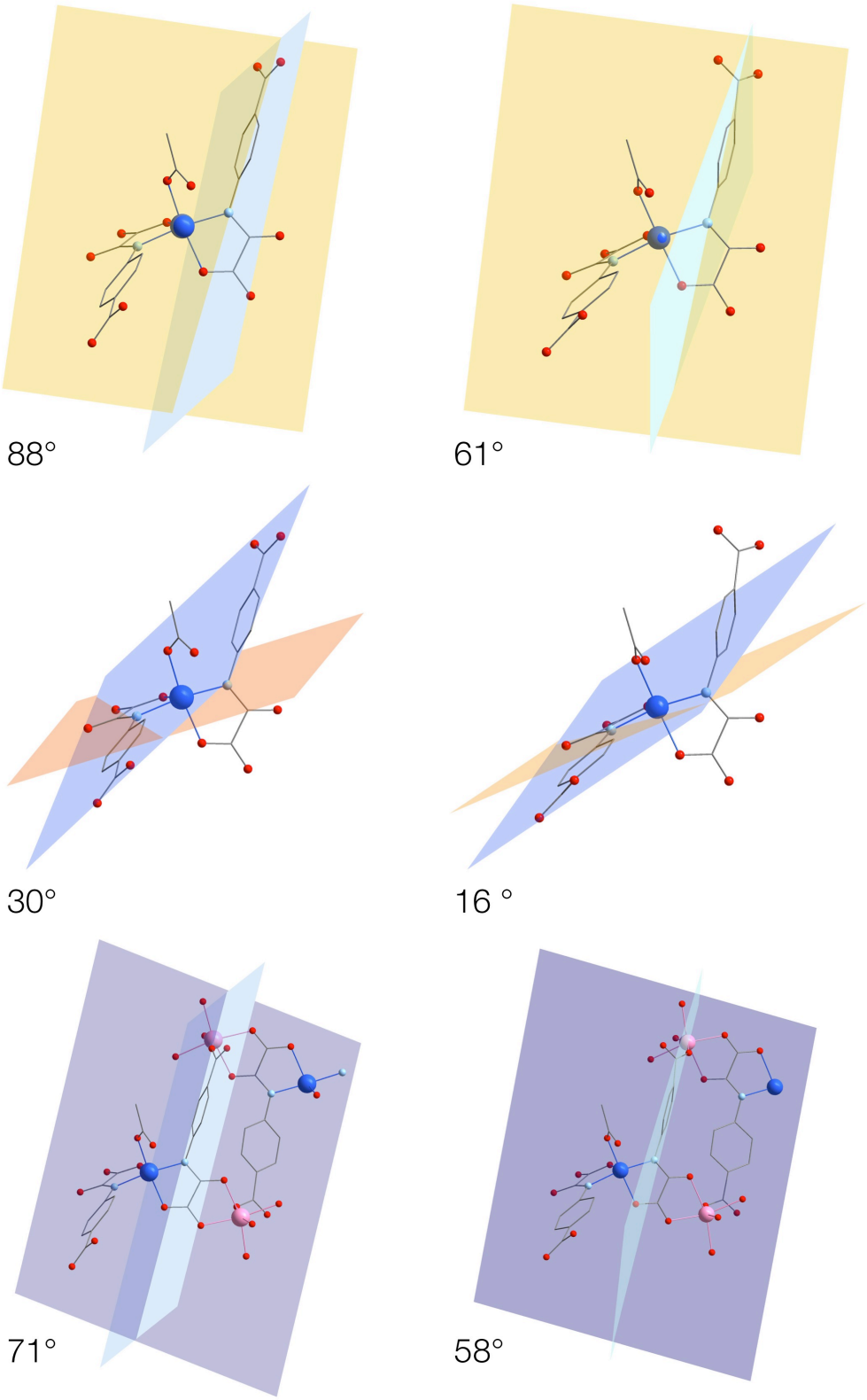


Figure S7. Representation and values of the dihedral angles in 1 and 1b. Phenyl ring/oxamate plane in the $[Cu(paba)_2(OAc)]^{5-}$ building complex and phenyl ring/phenyl ring along the brick-wall structure rung $\{Cu_2Mn_2(paba)_2\}$.

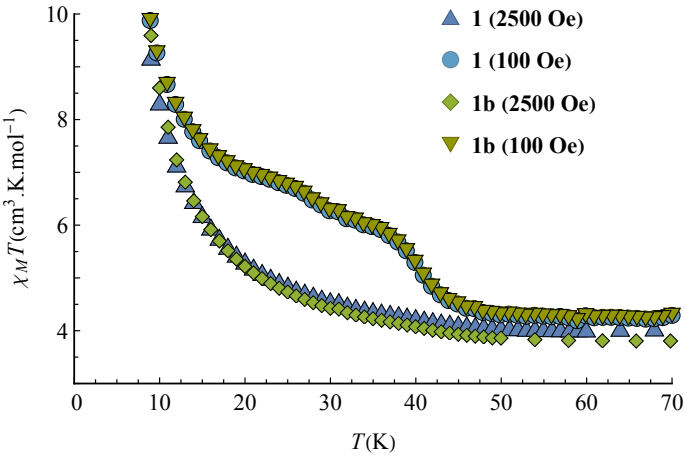


Figure S8. Temperature dependence of $\chi_M T$ for compounds 1 and 1b in the 70-10 K temperature range with applied fields of 100 Oe and 2500 Oe

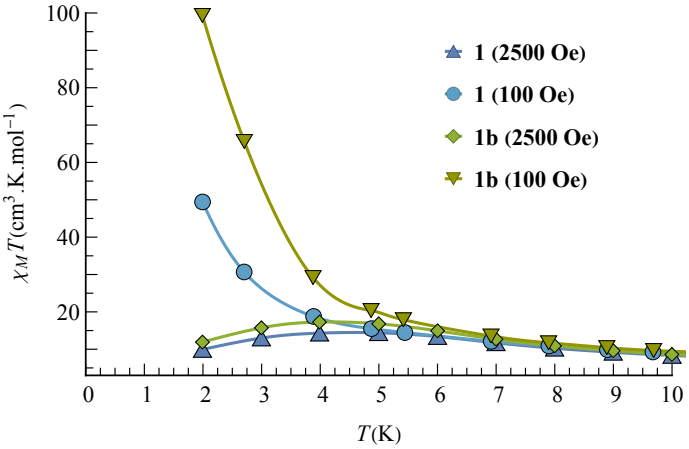


Figure S9. Temperature dependence of $\chi_M T$ for compounds 1 and 1b in the 10-2 K temperature range. The solid lines are guide for the eye

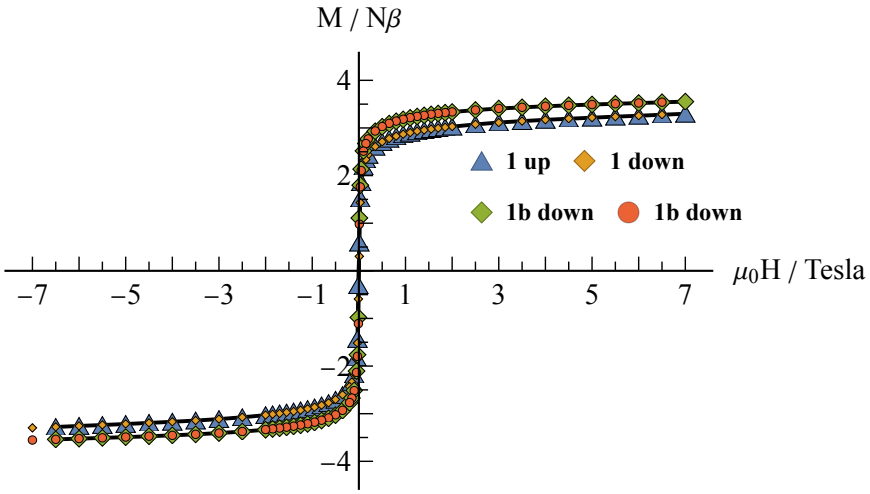


Figure S10. Hysteresis curves for compounds 1 and 1b at 2 K. The solid black lines are guide for the eye.

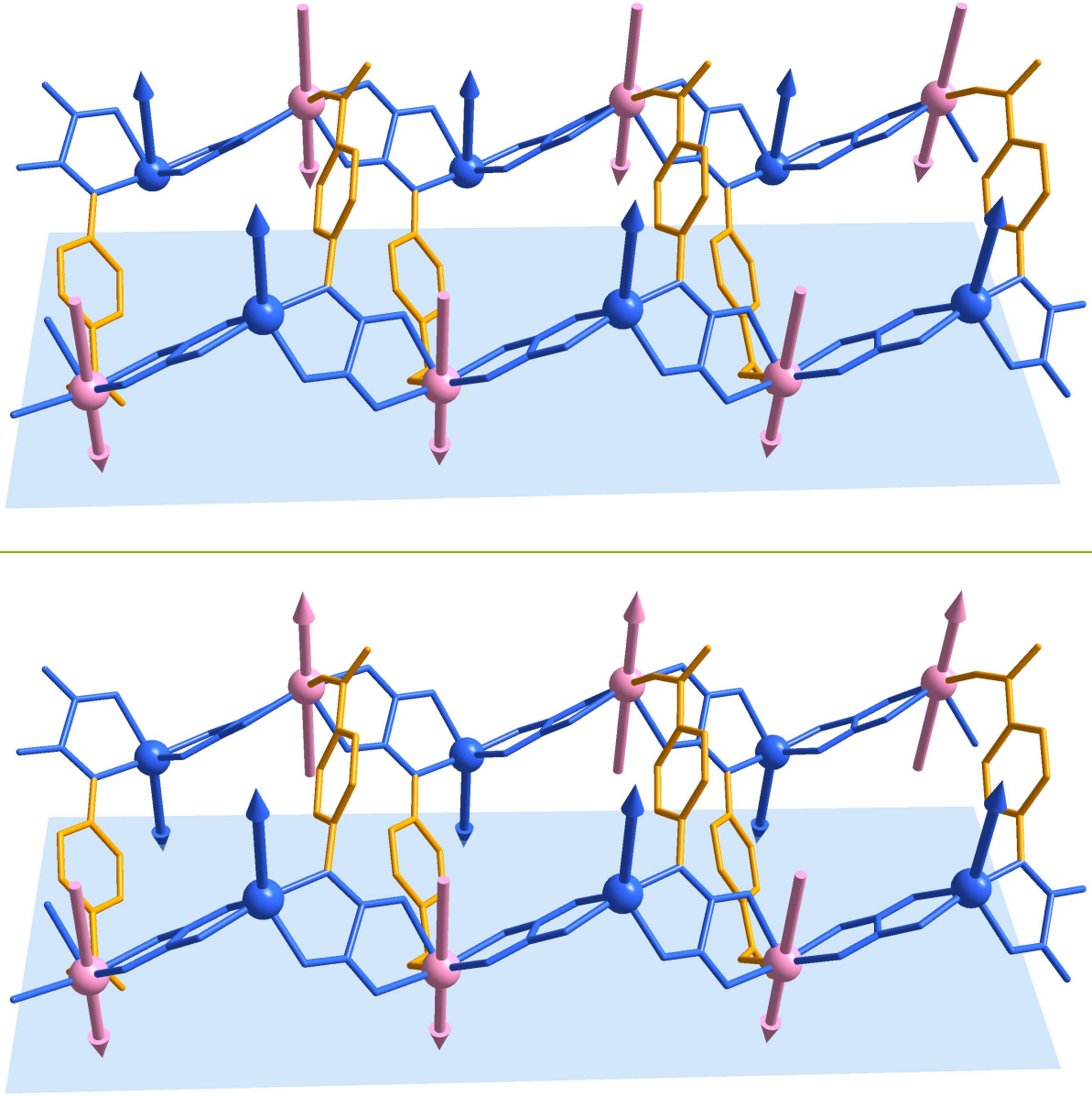

Figure S11. Representation of the possible coupling schemes in the 2D network. (top) AF through oxamato and phenylcarboxylato bridges. (bottom) AF through oxamato bridges and F through phenylcarboxylato bridges.


(1) Brese, N. E.; O'Keeffe, M. Bond-Valence Parameters for Solids. *Acta Crystallogr., Sect. B* **1991**, *47* (2), 192–197. https://doi.org/10.1107/S0108768190011041.

(2) O'Keeffe, M.; Brese, N. E. Bond-Valence Parameters for Anion-Anion Bonds in Solids. *Acta Crystallogr., Sect. B* **1992**, *48* (2), 152–154. https://doi.org/10.1107/S0108768191013083.